A physics-based statistical model for nanoparticle deposition

Cite as: J. Appl. Phys. **129**, 065303 (2021); https://doi.org/10.1063/5.0039861 Submitted: 08 December 2020 . Accepted: 22 January 2021 . Published Online: 08 February 2021

Bchara Sidnawi, Dong Zhou, Bo Li, and 🗓 Qianhong Wu







ARTICLES YOU MAY BE INTERESTED IN

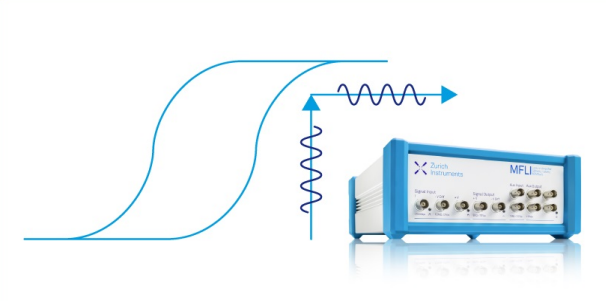
Contact-induced change of the bandgap of semiconductors of the wurtzite structure Journal of Applied Physics 129, 065702 (2021); https://doi.org/10.1063/5.0041029

Pressure-tailored synthesis of confined linear carbon chains

Journal of Applied Physics 129, 064302 (2021); https://doi.org/10.1063/5.0035854

Interface-dependent tunable elastic interface states in soft metamaterials

Journal of Applied Physics 129, 065305 (2021); https://doi.org/10.1063/5.0037592



Webinar How to Characterize Magnetic Materials Using Lock-in Amplifiers





Register now



A physics-based statistical model for nanoparticle deposition

Cite as: J. Appl. Phys. **129**, 065303 (2021); doi: 10.1063/5.0039861 Submitted: 8 December 2020 · Accepted: 22 January 2021 · Published Online: 8 February 2021







Bchara Sidnawi,^{1,2} Dong Zhou,^{1,3} Bo Li,^{1,3} and Qianhong Wu^{1,2,a)}

AFFILIATIONS

- Department of Mechanical Engineering, Villanova University, Villanova, Pennsylvania 19085, USA
- ²Cellular Biomechanics and Sport Science Laboratory, Villanova University, Villanova, Pennsylvania 19085, USA
- ³Hybrid Nano-Architectures and Advanced Manufacturing Laboratory, Villanova University, Villanova, Pennsylvania 19085, USA

ABSTRACT

In this study, a general theoretical framework is proposed to analyze particle deposition on a substrate, based on statistical and physical considerations. A model is developed in the context of the proposed framework to quantitatively predict the particle deposition on the substrate in terms of coverage evolution. Its validity was then verified by a dip coating experiment, where a polydimethylsiloxane substrate was periodically immersed in a sonicated graphene solution. An extension of the model was subsequently developed to describe the growth of the deposition thickness. The proposed framework's general applicability in any situation where particle deposition is taking place is expected to spur future endeavors in systematically characterizing film coating, drug delivery, and other processes involving particle deposition.

Published under license by AIP Publishing. https://doi.org/10.1063/5.0039861

I. INTRODUCTION

The deposition of particles onto surfaces is a widely observed phenomenon in both natural and industrial processes, such as inhalation,^{1,2} filtration,³ ash fouling on heat exchangers,^{4,5} drug delivery, dry deposition removing aerosols from the atmosphere, microcontamination control in the semiconductor industry,8 etc. Commonly, the particles are carried by a flow medium (e.g., air, water, etc.) and interact with the surface. They may deposit to or rebound from a surface depending on the interaction between the particles and the substrate. Understanding the particle deposition process is critical for solving many challenging problems, ranging from targeted drug delivery to the coating of nanoparticles for controllable manufacturing. Dip coating, for example, is a widely adopted method in advanced manufacturing, where a substrate is periodically immersed in a particle-carrying solution, prompting particle assembly on it. Applications of the said method include metal coating,⁹ textile coloring,¹⁰ food coating,¹¹ among many others. 12 With the fast development of nanotechnology, dip coating of nanomaterials (e.g., CNT, perovskite, and biomolecules) has been extensively studied and developed for strain sensors, 13 solar cells, 14,15 and biosensors. 16,17 In a recent study by our group, graphene flakes were assembled on a flexible substrate. 18 The observed assembly performance, in addition to its quick healing ability, shed

light on this method's potential for future flexible electronics applications.

A question that comes to mind is "What general physics govern the deposition process of suspended particles on a substrate?" The interactions of a single particle or multiple particles with substrates have been extensively studied on the microscopic level. Many of the studies are based on molecular dynamics simulations, which assume that a nanoparticle in the vicinity of the substrate surface has a probability of being adsorbed and a probability to rebound. 19 The rebound may occur when the particle velocity is above a critical velocity, which depends on the energy of adhesion between the particle and the surface.²⁰ Several models have been proposed to calculate the energy of adhesion, which include the Bradley-Hamaker (BH), Hertz, Johnson-Kendall-Roberts (JKR), Derjaguin-Muller-Toporov (DMT), and Maugis-Pollock (MP) models.²¹ Bouncing is also characterized by the coefficient of restitution which is the ratio between the particle's post-collision and incident velocities. The coefficient of restitution has been measured experimentally²² and calculated by molecular dynamics simulations.²³ Besides the MD simulation, the Lattice Boltzmann method (LBM), focusing on statistically predicting the interparticle and particle-substrate interactions, has been used to theoretically analyze particle deposition patterns resulting from the evaporation of

^{a)}Author to whom correspondence should be addressed: qianhong.wu@villanova.edu. Tel.: +1-610-519-8969

colloidal drops²⁴ and soot deposition distributions in diesel particulate filters (DPFs).²⁵ Particulate fouling has also been computationally investigated in porous metal foam heat exchangers via a finite volume-discrete element couple method²⁶ and on dimpled heat transfer surfaces both numerically and experimentally.²⁷ The effect that the thickness of a plate in a parallel airflow has on particle deposition velocity has been studied experimentally and numerically.²⁸ Trajectory analysis of individual particles within an impinging jet has been performed to study their deposition on heterogeneous substrates with micropatterned surface charge.²⁹ The deposition of electrospun nanofibers on both moving and stationary substrates, on the other hand, has been simulated.³⁰ The driving forces considered in that study were particle-particle Coulomb force, surface tension, electric-field-induced force, and viscoelastic forces. Friction and gravity were neglected. Elaborate stochastic and statistical models for particle deposition in turbulent flows have also been developed. 31,32 An extensive Monte Carlo model for particle deposition has been developed, using a novel adherence-potential barrier.³³ On the other hand, another classical theory, Langmuir's theory of site-specific molecular adsorption³⁴ was first introduced to describe the adsorption of gas molecules on solid surfaces, under different pressure and temperature conditions. However, the theory focuses on chemical interactions between the adsorbed particles and the substrate, and describes molecular layers of deposits at specific binding sites.

Review of the literature indicates that, despite of extensive studies about the mechanism driving the nanoparticle deposition, there are studies mainly on a case by case basis. In any circumstance, whether a particle will deposit on a substrate solely depends on the substrate-particle-medium interfacial energies, and the particle's incident velocity vector upon impact. Since the number of particles is usually too big to consider every single one of them, and the flow field in the carrying medium is rarely enough to infer the particles' velocity distribution, much of this phenomenon is stochastic in nature. In other words, a general theoretical framework tying the macroscopically observed coverage and thickness growth rates to the microscopic statistical and physical properties of the particles surrounding a substrate is lacking in the literature. The paper presented herein is aimed to fill in the knowledge gap by developing a theoretical framework, based on statistical and physical considerations, to characterize particle deposition in any general settings. As a sample system to demonstrate the theory, a dip coating scenario is specifically considered. A deposition model is first developed and validated experimentally, where a polydimethylsiloxane (PDMS) substrate is cyclically immersed in a sonicated graphene solution. An extension of the model is subsequently developed to reflect the feature of multilayered deposition and hence the growth of the deposition thickness.

II. COVERAGE MODEL

Figure 1 depicts a substrate being periodically immersed (along the y-direction) into a solution with dispersed nanoparticles, as an example of the general problem being examined. Consider a particle approaching the substrate at a certain velocity V. The velocity vector has a component that is normal to the substrate (w), and another that is parallel to it (s), which can also be decomposed

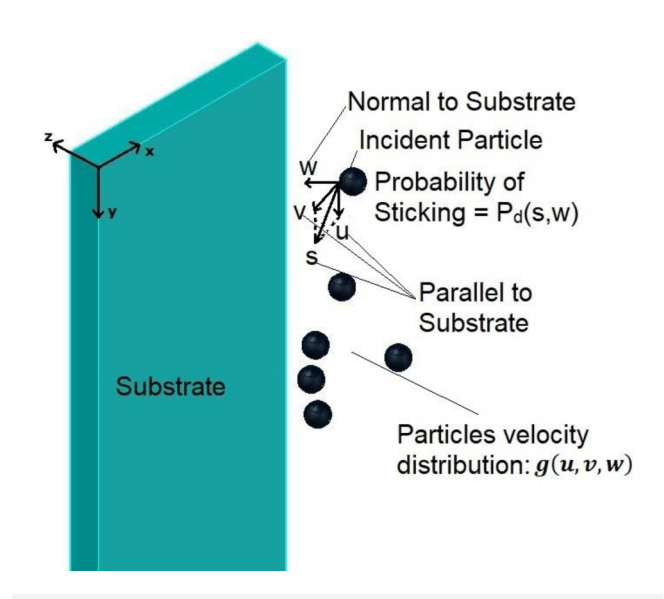


FIG. 1. A schematic showing detailed look at a particle approaching the substrate.

to u and v. As a result of surface interactions, a portion of those particles deposit on the substrate, eventually forming a thin film. When the type and material for both the particle and the substrate are determined, one would expect that the probability of the particle depositing on the substrate after colliding with it, P_d , is a certain function of the head-on and sideways components of the particle's velocity: $P_d = P_d(s, w)$.

Consider a suspension of those particles being irradiated with external forces, e.g., sound waves. The velocity distribution of particles would be a certain probability density function g(u, v, w) (s^3m^{-3}). In other words, the probability of a particle's velocity being within (u + du, v + dv, w + dw) is $g \, du \, dv \, dw$.

Now take a patch of exposed area, dA on the substrate. After an infinitesimal amount of time dt, this patch will have been hit by a certain number of particles, dN_h . Evidently, dN_h would include particles of all possible velocity vectors heading toward the substrate. However, before the collision, for a particle with a head-on velocity w to hit dA within dt, its distance away from the substrate cannot exceed wdt. This means that all the particles that will hit dA with a head-on velocity in the vicinity of w are contained within an infinitesimal volume, $\delta V = w dt dA$. Therefore, for a given particle concentration, $n_p(m^{-3})$, δN_h , which exclusively counts the particles hitting within a certain velocity vector, V, can be obtained as

$$\delta N_h = w \ dt \ dA \ n_p \ g(u, v, w) dw \ du \ dv. \tag{1}$$

Only a fraction of δN_h , which we denote as δN_d , will stick and end up depositing on dA. This fraction is the probability $P_d(s, w)$, where $s = \sqrt{u^2 + v^2}$. Hence,

$$\delta N_d = w \ dt \ dA \ n_p \ g(u, v, w) P_d(s, w) dw \ du \ dv. \tag{2}$$

To obtain the infinitesimal number of particles that deposited on dA within dt, the above expression is integrated over half the velocity space (the other half corresponding to the particles moving away from the substrate),

$$dN_d = \int_{-\infty}^{\infty} \int_{-\infty}^{\infty} \int_{0}^{\infty} w \ dt \ dA \ n_p \ g(u, v, w) P_d(s, w) dw \ du \ dv.$$
 (3)

Since the integration is performed over the velocity space, dA and dt can be brought outside, along with n_p . If m (kg) is the particle's mass, then the solution concentration C (kg/m^3) is $C = mn_p$. Hence, the frequency $f(m^{-2}s^{-1})$ of particle deposition on the exposed area of the substrate is obtained as

$$f = \frac{1}{dA} \left(\frac{dN_d}{dt} \right) = \frac{C}{m} \int_{-\infty}^{\infty} \int_{-\infty}^{\infty} \int_{0}^{\infty} wg(u, v, w) P_d(s, w) dw \ du \ dv.$$
 (4)

With the types and materials of the particle solutions and substrates being known, and the experimental conditions set, $P_d(s, w)$, and g(u, v, w) are then determined. This shows that f is a linear function of C,

$$f = \alpha C,$$
 (5)

where α is the definite integral

$$\alpha = \frac{1}{m} \int_{-\infty}^{\infty} \int_{-\infty}^{\infty} \int_{-\infty}^{\infty} wg(u, v, w) P_d(s, w) dw \ du \ dv. \tag{6}$$

While it may be argued that physical intuition can be enough to assume the truth of Eq. (5) and just proceed from there, the development above [Eqs. (1)-(6)] was deemed instructive for two reasons. The first is that it rigorously validates this intuitive inference, once and for all. The second is that the explicit general form of α , stated by Eq. (6), quantitatively elucidates the interplay between the factors affecting the deposition performance, namely, experimental conditions (e.g., sonication condition) through g(u, v, w), and the choice of the substrate-solution pairing [through $P_d(s, w)$]. For a specific situation, different mechanisms driving the particle deposition and growth, including but not limited to van der Waals attractive force, electrostatic double layer force, hydrodynamic drag force, lift force, buoyancy force, and Brownian motions, etc. would be reflected in the deposition probability, P_d , and the velocity distribution, g, which, in turn, affect the parameter α in Eq. (6). Therefore, any future studies involving wellcontrolled experiments or molecular dynamics simulations, where the specific molecular interactions could be accurately estimated to infer P_d and g, can use Eq. (6) to obtain the adsorption rate. In the current study, these collective effects will be inferred from a sample dip coating experiment, by finding the appropriate value of α that provides the best fit between the experimentally observed coverage rate and their theoretical counterpart.

Next, we shall investigate the substrate's coverage evolution. Although a particle depositing on top of another that has already occupied a spot on the substrate is a real possibility, this would not affect the coverage status of that spot. Once it receives a particle, it will always appear as occupied when viewed from the top. Since α is related to the deposition frequency on the exposed fraction of the substrate, exclusively, the following development will be useful for inferring α from the experimentally observed local deposition described later in this paper. As detailed in Sec. III, the obtained optical images of the substrate only provide a top view through which a given spot can be judged as either occupied or vacant.

Let F be the exposed fraction of an area of the substrate where the nanoparticle surface density is δ (kg/m²), and a_p (m²) be the area occupied by one particle on the substrate. As we have already established that stacked particles do not affect the coverage status of a given location, δ will refer to the surface density corresponding to just one layer of particles. The exposed fraction, F would then be obtained as

$$F = 1 - \frac{\delta a_p}{m}. (7)$$

This yields the rate of change of surface density at the subtrate,

$$\frac{\partial \delta}{\partial t} = \alpha C m \left(1 - \frac{a_p}{m} \delta \right). \tag{8}$$

Equation (8) will now be solved for each vertical location, *y*, during one dipping cycle of the substrate. Defining the dimensionless parameters,

$$\delta^* = \frac{a_p}{m} \delta, \quad t^* = \alpha C_0 a_p t, \quad C^* = \frac{C}{C_0}, \quad y^* = \frac{y}{L}.$$
 (9)

Equation (8) becomes (for the ith dip)

$$\frac{\partial \delta^*}{\partial t^*} = C_{i-1}^* (1 - \delta^*). \tag{10}$$

Note that for one layer of nanoparticles, $\frac{m}{a_p}$ is the upper bound of δ , making $\delta^* = 1 - F$ [Eqs. (7) and (9)], the covered fraction itself. Let T(y) be the immersion time spent by a vertical location, y, on the substrate (Fig. 1). The solution to Eq. (10) during the ith dip gives the evolution of the nanoparticle surface density during that dip. For $0 < y^* < 1$, and $0 < t^* < T^*(y^*)$ (top end: $y^* = 0$, bottom end: $y^* = 1$),

$$\delta_{i}^{*}(y^{*}, t^{*}) = 1 - (1 - \delta_{i-1}^{*}(y^{*}, T^{*}(y^{*})))e^{-C_{i-1}^{*}t^{*}}.$$
 (11)

Letting W, L, and V be the substrate's width, immersed length, and the solution's volume, respectively, C_i can be obtained by integrating the mass captured by the substrate during the previous dip,

$$C_{i} = C_{i-1} - \frac{W}{V} \int_{0}^{T(y)} \frac{\partial \delta_{i}}{\partial t} dt dy, \qquad (12a)$$

or in dimensionless terms,

$$C_{i}^{*} = C_{i-1}^{*} - \frac{WLm}{a_{p}VC_{0}} \int_{0}^{T^{*}(y^{*})} \frac{\partial \delta_{i}^{*}}{\partial t^{*}} dt^{*} dy^{*}.$$
 (12b)

Equations (11) and (12b) should be applied to successive dips to obtain the evolution of $\delta^*(y^*, t^*)$. For illustrative purposes, we will consider an example in which the immersion time is of a linear shape: $T^*(y^*) = ay^*$, applying Eq. (11) to successive dips shows that the surface density distribution by the end of the *i*th dip looks like

$$\boldsymbol{\delta}_{i}^{\star} = 1 - e^{-k_{i}y^{\star}},\tag{13}$$

where $k_i = a \sum_{j=0}^{i-1} C_j^*$. From Eq. (12b), the solution concentration after the *i*th dip, C_i^* is obtained from C_{i-1}^* as

$$C_i^* = C_{i-1}^* + \frac{WLm}{a_p V C_0} \left[\frac{1}{k_i} (1 - e^{-k_i}) - 1 \right].$$
 (14)

Figure 2 shows the surface density after different numbers of dips. The chosen parameter values are a=0.4 and $\frac{wLm}{a_pVC_0}=0.01$ (again, for demonstration purposes). Note how with further dipping cycles, the distribution gradually becomes flat, showing an eventual indifference to the immersion time, which is more apparent at lower vertical locations (greater values of y^* and, therefore, longer residence times) as the substrate becomes close to saturation.

III. EXPERIMENT

To validate the coverage model, a sono-assisted surface energy-driven assembly mechanism is developed to assemble graphene (average diameter of $\sim 5 \, \mu \mathrm{m}$ and average thickness of approximately 6–8 nm, and a density of 2300 kg cm⁻³, XGSciences) flakes on polymer substrates. ¹⁸ The PDMS was prepared by mixing

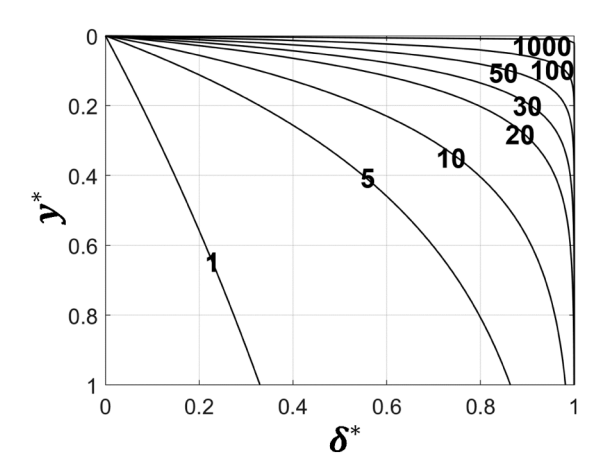


FIG. 2. Evolution of the surface density distribution after the *i*th dip, where i = 1, 5, 10, 20, 30, 50, 100, and 1000.

the monomer and crosslink agents with a volume ratio of 10:1. The as-mixed PDMS was cast into a square Petri dish and cured at room temperature for one week before the assembly. An unfavorable solvent (i.e., water) for both graphene and PDMS is used to drive the assembly of graphene on the PDMS surface. The assembly was done using a graphene solution (0.5 mg ml⁻¹) and PDMS substrate under the sonication (20 kHz, 0.3 W cm⁻²). Under the effect of sonication, the dispersion of graphene can be maintained, and the assembly process can be significantly facilitated. In order to mimic the relative motion between the particle media and the substrate, a customized dip coating system is used, and the diagram is shown in Figs. 3(a) and 3(b). The setup is mainly constructed by a customized slider-crank mechanism composed of 3D printed parts and is driven by a linear DC motor with a fixed angular speed of 60 rpm. A representative displacement vs time curve in one dipping cycle is shown in Fig. 3(c). Intuitively, the actual assembly time (the time of substrate immersed in water) is related to the dipping time. In each dipping cycle with 1 s period, the actual assembly time is 0.5 s. Due to the bottom part of the substrate being immersed in the solution for longer than the top, the deposition efficiency can be expected to change with the distance from the top of the substrate, leading to a thickness gradient. Under the same deposition condition, the coverage increases with the assembly time, which is reflected in the optical images [Fig. 3(d)]. The coverage increases from top to bottom in the same sample. In the same position, increased coverage can be found with increased dipping times, i.e., assembly time.

The quantitative coverage was obtained by calculating the ratio between the deposited graphene area and the overall area and summarized in Fig. 4 The length of the substrate (3 cm) is normalized to 1 and represented by y^* . Figure 4 shows an increasing coverage for greater values of y^* , due to their corresponding longer residence time during a given dip. As the number of dips grows, the coverage approaches saturation.

IV. MODEL VALIDATION

Typically, the particle build-up on the substrate plateaus at a thickness of a couple hundred nanometers, amounting to a negligible mass adsorbed from the nano-solution. With the number of particles in the solution at which the experiment starts off, the final particle concentration remains practically unchanged. Therefore, to experimentally obtain the value of α in the context of the coverage model in Sec. II, the concentration, C, was assumed to be C_0 throughout all 100 dipping cycles. As will be outlined in Secs. IV A and IV B, the value of α will first be extracted based on the observed coverage distribution resulting from a certain number of dipping cycles. The calculated value will then be used to predict the coverage resulting from the other numbers of dips.

A. Extraction of α

With a constant concentration, according to the coverage model, the substrate coverage distribution, $\delta_i^*(y^*)$, after the *i*th dip, simplifies to Eq. (15), by solving Eq. (10) for $C^*=1$, and

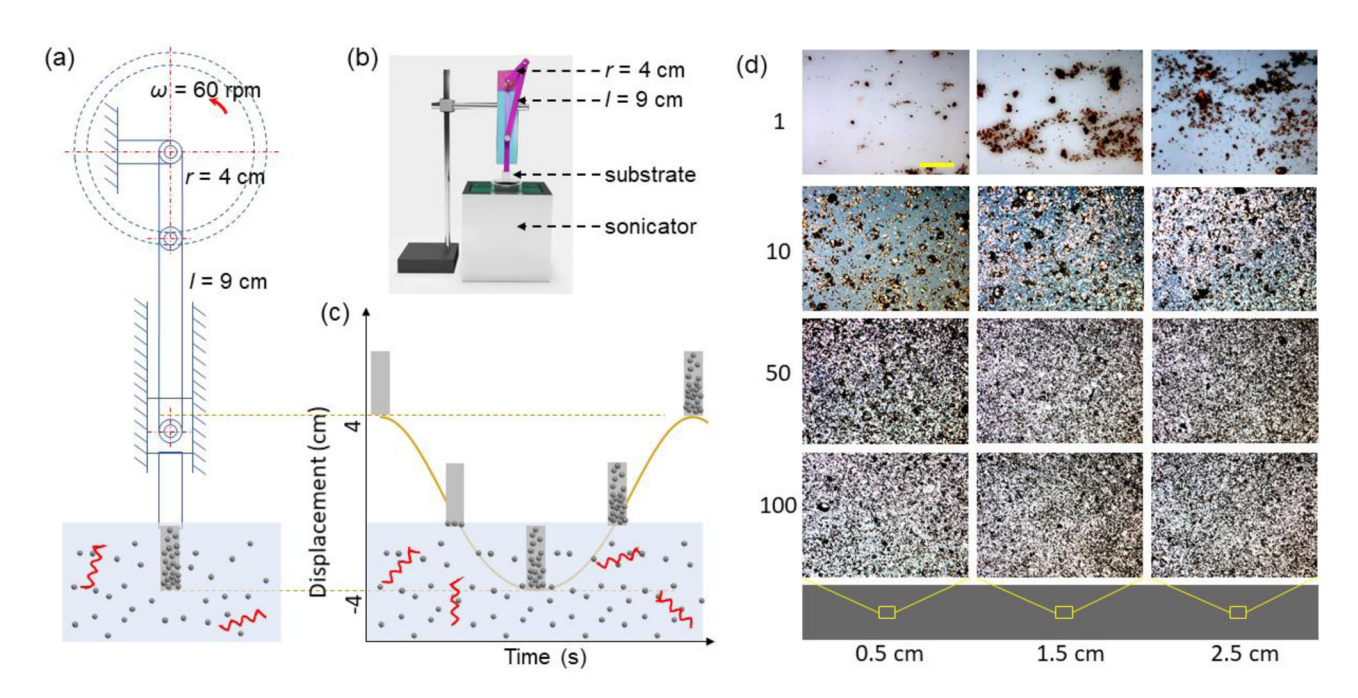


FIG. 3. (a) Schematic of the customized dip coating system. (b) Real experimental setup image. (c) Schematic showing the moving trajectory of the substrate in one dipcoating cycle. (d) Optical images of the substrate at three vertical locations, y = 0.5 cm, 1.5 cm, and 2.5 cm, after the *i*th dipping cycle, i = 1, 10, 50, 100, respectively. The y axis is measured from the top of the substrate (Fig. 1). The scale bar is $100 \, \mu \text{m}$.

substituting t^* by the cumulative immersion time, $iT^*(y^*)$,

$$\delta_{i}^{*}(y^{*}) = 1 - e^{iT^{*}(y^{*})}. \tag{15}$$

Since $T^*(y^*) = \alpha C_0 a_p T(y^*)$, the value of α is embedded in the appropriate inverse of the time scale, $P(s^{-1}) = \alpha C_0 a_p$, which brings $\delta_i^*(y^*)$ closest to the observed coverage distribution (Fig. 4), for a

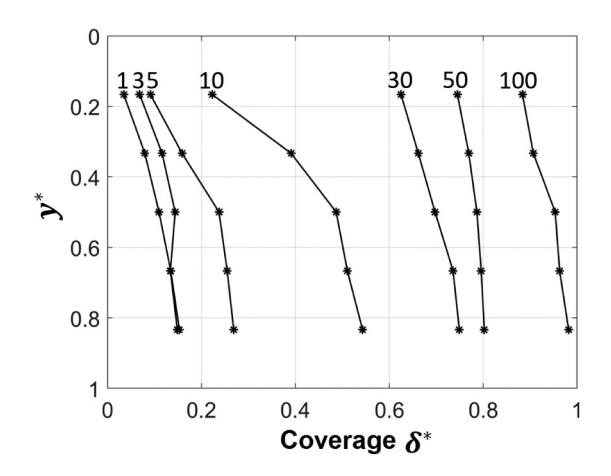


FIG. 4. Coverage results for different numbers of dips as a function of vertical location.

given value of i. The residence time, T(y), corresponding to the geometry and speed settings of the crank-slider mechanism (Fig. 3) can be obtained as

$$T(y) = \frac{2}{\omega} \cos^{-1} \left(1 + \frac{y(y-2l)}{2r(r+l-y)} \right).$$
 (16)

The number of dips on which the calculation of P was based is i=30, for reasons that will be discussed in Sec. IV B. The value of P that scaled T(y), and generated a distribution, $\delta_{30}^*(y^*)$, that was closest to its observed counterpart (had the least RMS error), was $P=0.32\ s^{-1}$. This implies a value of $\alpha=\frac{P}{C_0a_0}$.

B. Predictions of coverage distribution based on α

The value of P that was calculated based for i=30, was used to obtain $T^*(y^*)$, which was substituted in Eq. (15) to predict $\delta_i^*(y^*)$, for the other values of i (i=1,3,5,10,50,100). Before getting into the details of the comparison results shown in Fig. 5, three significant sources of uncertainty should be pointed out, two of which led to the choice of i=30 dips for the calculation of P. The first is statistical significance. Inferring the value of P (and therefore α), from a small number of dips, makes an inaccurate assumption that the observed coverage resulting from those dips would be representative of the actual deposition rate that is directly related to α . The second source of uncertainty is the hindering effect. The model is developed in the context of a smooth continuum of deposition density, where every spot on the substrate is visualized as part occupied and another that is vacant. However,

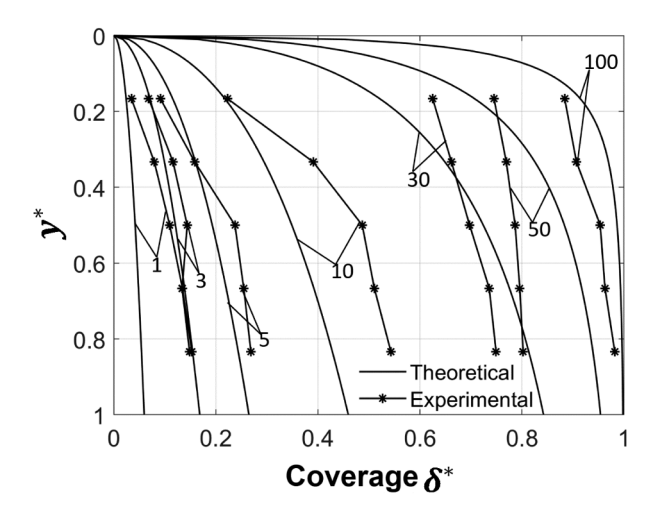


FIG. 5. Predicted vs experimentally observed coverage.

the physical particles tend to form local aggregates. When a vacant location on the substrate happens to be surrounded by those aggregates (Fig. 3), it becomes more difficult for an incoming particle to occupy it. Hence, while the coverage distribution resulting from a greater number of dips is statistically preferable for the calculation of P, the prevalence of the hindering effect when the coverage is too dense (i too large) will lead to an underestimate of P (and consequently α). Therefore, as a compromise, the intermediate value of i (i=30) was chosen. The third source of uncertainty resides in the processing of the optical images to estimate the coverage. As can be seen in Fig. 3, the brightness signature of the deposits is mostly bipolar, where some stand out as bright regions while others as dark. This makes the thresholding for the disjoint ranges of brightness that are relevant to the deposits a bit challenging, thereby introducing inevitable errors in the coverage estimation.

Based on i = 30, we theoretically predicted that coverage of nanoparticles on the substrate at different locations and for different numbers of dips. The theoretical predictions agree reasonably well with the experimental data, Fig. 5, despite all the uncertainties explained above. Since the hindering effect is not completely absent after 30 dips, the prediction tends to underestimate the coverage corresponding to smaller numbers of dips, where hindering is not as prevalent. The relatively greater deviation corresponding to the coverage after 1 dip can be attributed to the problem of statistical significance where the coverage resulting from the 1-dip experiment performed one time, can significantly fluctuate around the predicted average. The stark difference observed for 10 dips may be attributed to the experimental coverage estimation errors due to the bipolar brightness signature of the deposits in the optical images as can be seen in the row corresponding to 10 dips in Fig. 3. Even the trend of the experimental coverage distribution corresponding to 10 dips looks quite different than the others. Since hindering would be more severe for greater numbers of dipping cycles, the prediction overestimates the coverage for 50 and 100 dips. Overall, the theoretical model captures the general behavior of the particle deposition and its spatial distribution.

V. THICKNESS GROWTH MODEL: MULTIPLE LAYER DEPOSITION

Based on the validated coverage model, which quantifies the interaction between the particles and the substrate, through the parameter α , a model for the thickness growth will be proposed. In this model, both particle-substrate and particle-particle interactions are represented through a value of α that varies with the distance z from the substrate. As mentioned earlier in Sec. IV, the total mass that ends up depositing on the substrate is so small that the solution concentration is left practically unchanged. The selflimiting thickness growth indicates a decreasing deposition probability with increasing thickness, which points to a decreasing value of α (eventually vanishing). To model this process in a consistent theoretical framework, each level (z) above the substrate is visualized as having all its points occupied by parts of an infinitesimal slice (dz) of the depositing material. To put it differently, at every instant during immersion, the semi-infinite line standing on each immersed point of the substrate has growth occurring on each of its points, at decreasing rates further from the substrate. Integrating the incremental surface concentrations along this semi-infinite line would then yield the total surface concentration (δ) at its corresponding location on the substrate. Equation (8) will, therefore, be applied to the incremental counterparts of δ and m, denoted as $\hat{\delta}$ and \hat{m} , respectively, with the concentration as a constant for the reason pointed out earlier,

$$\frac{\partial \hat{\delta}}{\partial t} = \alpha(z) C_0 \hat{m} \left(1 - \frac{a_p}{\hat{m}} \hat{\delta} \right). \tag{17}$$

Nondimensionalizing as follows:

$$\hat{\delta}^* = \frac{a_p}{m} \hat{\delta}, \qquad t^* = \alpha_0 C_0 a_p t, \qquad \alpha^* = \frac{\alpha}{\alpha_0}, \qquad T^*(y^*)$$

$$= \alpha_0 C_0 a_p T(y), \qquad \hat{m}^* = \frac{\hat{m}}{m} = \frac{dz}{h}, \qquad z^* = \frac{z}{z_0}. \tag{18}$$

where α_0 , h, and z_0 are the value of α at the substrate's level, the particle's height, and a general height scale, respectively, Eq. (17) becomes

$$\frac{\partial \hat{\boldsymbol{\delta}}^*}{\partial t^*} = \alpha^*(z^*)\hat{m}^* \left(1 - \frac{\hat{\boldsymbol{\delta}}^*}{\hat{m}^*}\right),\tag{19}$$

to which the solution is

$$\hat{\delta}^* = \hat{m}^* (1 - e^{-t^* \alpha^* (z^*)}). \tag{20}$$

Recognizing that Eq. (20) describes infinitesimal quantities, the dimensionless surface distribution is then integrated as

$$\delta^* = \frac{z_0}{h} \int_0^\infty (1 - e^{-t^* \alpha^* (z^*)}) dz^*. \tag{21}$$

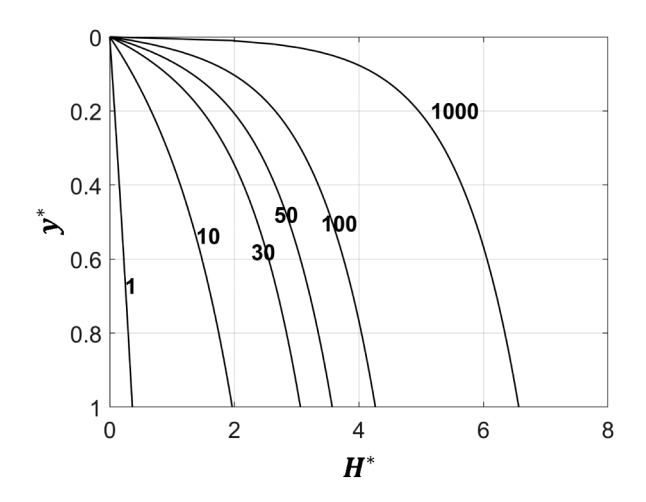


FIG. 6. Evolution of the deposition profile over 1000 dipping cycles.

The deposits thickness distribution would then be $H = \frac{\delta}{\rho}$, where ρ is the deposits density. Hence,

$$H^* = \frac{H}{z_0} = \frac{h}{z_0} \delta^* = \int_0^\infty (1 - e^{-t^* \alpha^*(z^*)}) dz^*. \tag{22}$$

On a side note, the convergence of the integral in Eqs. (21) and (22) is not unconditional. Functional forms of $\alpha^*(z^*)$ that keep the function $\psi(z^*) = z^*p(1-e^{-\alpha^*(z^*)})$ bounded as $z^* \to \infty$, for p > 1, guarantee convergence. Substituting t^* in Eq. (22) by the dimensionless residence time, $T^*(y^*)$ multiplied by the number of dipping cycles, i, the thickness distribution after the ith dip, $H_i^*(y^*)$, is then obtained as

$$H_i^*(y^*) = \int_0^\infty (1 - e^{-iT^*(y^*)\alpha^*(z^*)}) z^*. \tag{23}$$

In the formulation above, $\alpha(z)$ is a general decreasing function, vanishing as $z^* \to \infty$, To get a sense of what Eq. (23) predicts, an exponential form is explored: $\alpha(z) = \alpha_0 e^{-\beta z}$, which means $\alpha^*(z^*) = e^{-z^*}$ where $z^* = \beta z$ (making the chosen height scale $z_0 = \frac{1}{\beta}$). The figure shows that the thickness distribution when α is exponential, and $T^*(y^*) = ay^*$, for a = 0.4.

Despite the evolving profile in Fig. 6 tending toward a flat slope after infinite dipping cycles, indicating an ever-slowing growth rate, the growth itself (H^*) is not bounded. This can be seen in Eq. (22) where if $\alpha^*(z^*)$ is not exactly 0, H^* will keep increasing for arbitrarily longer immersion periods. In reality, however, there is a cutoff growth thickness where deposition completely stops, and beyond which α is exactly 0, thereby making H^* bounded at 1 (by choosing the height scale, z_0 , as the cutoff thickness). Future studies can experimentally investigate the cutoff thickness in different conditions, from which the functional form of $\alpha(z)$ can be inferred using this model. It is noticed that the growth model presented herein is not validated experimentally due to the limitation of our experiments. Nevertheless, since the growth model is an

extension of the coverage model which has been validated experimentally, its validity can be inferred from that of the latter with reasonable confidence. An on-going experimental study is performed by our group which would allow us to directly validate the growth model.

VI. CONCLUSION

In this paper, a statistical, physics-based, theoretical framework was proposed, in which a model for particle deposition on a substrate was developed. The part of the model concerned with deposition coverage was tested against experimental results from a dip coating setup where a PDMS substrate is cyclically immersed in a sonicated graphene solution. Optical images of the substrate at different vertical locations, after several numbers of dips were obtained and processed for the covered fraction. The coverage data corresponding to 30 dipping cycles were used to infer the value of the parameter α , which in this study, was shown to quantify the substrate-nanoparticle interaction for given sonication conditions. The inferred value was substituted in the coverage model to predict the coverage profiles corresponding to the other numbers of dips. Overall, the predictions compared well with experimental data, despite anticipated discrepancies attributed to statistical significance, image processing uncertainties, and the hindering effect for dense coverage. The model was extended to accommodate the growth of deposition thickness resulting in sensible theoretical results, thereby setting the stage for future efforts to experimentally determine α 's thickness dependence.

The paper presented herein provides a unifying general theoretical framework to describe particle deposition in any setting, by rigorously relating the microscopic physical and statistical properties of particle-substrate interactions to the macroscopically observed coverage rate. The details of microscopic mechanisms driving particle deposition are not the crux of what this paper is concerned with. Studies examining those on a case by case basis are abundantly available in the literature. However, theories describing macroscopic observations of particle coverage and film growth are lacking in the literature, despite their fundamental importance. The current paper fills in this knowledge gap. Specifically, Eq. (6) is a general exact expression relating the macroscopically observed adsorption rate to the statistical description of particles in the vicinity of the substrate. In any process involved with nanoparticle deposition on a substrate, no matter what type of physical or chemical interactions are involved, their effects, as reflected in the deposition probability, P_d , and the velocity distribution, g, will affect the parameter α in Eq. (6), which is used to predict the deposition performance on the macroscopic level. Being reminiscent of the famous Langmuir's theory of site-specific molecular adsorption, 34 the parameter α characterizing the adsorption rate can serve as the adsorption coefficient in Langmuir's kinetic equation.

ACKNOWLEDGMENTS

This research was supported by the National Science Foundation (NSF) under Grant Nos. 1511096 and 2003077. D.Z. and B.L. also acknowledge financial support from the Startup fund of the Villanova University.

DATA AVAILABILITY

The data that support the findings of this study are available from the corresponding author upon reasonable request.

REFERENCES

- ¹C. Kleinstreuer and Y. Feng, "Computational analysis of non-spherical particle transport and deposition in shear flow with application to lung aerosol dynamics—A review," J. Biomech. Eng. 135, 021008 (2013).
- ²Z. F. Tian, K. Inthavong, and J. Y. Tu, "Deposition of inhaled wood dust in the nasal cavity," Inhal. Toxicol. **19**, 1155–1165 (2007).
- ³C. R. O'Melia, "Pretreatment, and performance in water filtration," ASCE 3, 874–890 (1986).
- ⁴Y. Cai *et al.*, "Modeling of ash formation and deposition processes in coal and biomass fired boilers: A comprehensive review," Appl. Energy **230**, 1447–1544 (2018).
- ⁵U. Kleinhans, C. Wieland, F. J. Frandsen, and H. Spliethoff, "Ash formation and deposition in coal and biomass fired combustion systems: Progress and challenges in the field of ash particle sticking and rebound behavior," Prog. Energy Combust. Sci. 68, 65–168 (2018).
- ⁶P. Charoenphol, P. J. Onyskiw, M. Carrasco-Teja, and O. Eniola-Adefeso, "Particle-cell dynamics in human blood flow: Implications for vascular-targeted drug delivery," J. Biomech. 45, 2822–2828 (2012).
- ⁷E. W. Emerson *et al.*, "Revisiting particle dry deposition and its role in radiative effect estimates," Proc. Natl. Acad. Sci. U.S.A. 117, 26076–26082 (2020).
- ⁸T. H. Van Steenkiste *et al.*, "Kinetic spray coatings," Surf. Coat. Technol. 111, 62–71 (1999).
- ⁹M. Seo, Y. Akutsu, and H. Kagemoto, "Preparation and properties of Sb-doped SnO₂/metal substrates by sol-gel and dip coating," Ceram. Int. **33**, 625–629 (2007). ¹⁰B. Mahltig and T. Textor, "Combination of silica sol and dyes on textiles," J. Sol-Gel Sci. Technol. **39**, 111–118 (2006).
- ¹¹B. E. Meza, J. M. Peralta, and S. E. Zorrilla, "Rheological properties of a commercial food glaze material and their effect on the film thickness obtained by dip coating," J. Food Process Eng. 38, 510–516 (2015).
- ¹²L. E. Scriven, "Physics and applications of DIP coating and spin coating," MRS Proc. 121, 717 (1988).
- ¹³G. Cai et al., "Flexible and wearable strain sensing fabrics," Chem. Eng. J. 325, 396–403 (2017).
- ¹⁴H. C. Liao et al., "Enhanced efficiency of hot-cast large-area planar perovskite solar cells/modules having controlled chloride incorporation," Adv. Energy Mater. 7, 1601660 (2017).
- ¹⁵G. Rajesh, N. Muthukumarasamy, E. P. Subramaniam, S. Agilan, and D. Velauthapillai, "Synthesis of Cu₂ZnSnS₄ thin films by dip-coating method without sulphurization," J. Sol-Gel Sci. Technol. 66, 288–292 (2013).
- ¹⁶M. S. Crosley and W. T. Yip, "Kinetically doped silica sol-gel optical biosensors: Expanding potential through dip-coating," ACS Omega 3, 7971–7978 (2018).

- ¹⁷S. Kumar et al., "Reduced graphene oxide modified smart conducting paper for cancer biosensor," <u>Biosens. Bioelectron.</u> 73, 114–122 (2015).
- ¹⁸D. Zhou et al., "Sono-assisted surface energy driven assembly of 2D materials on flexible polymer substrates: A green assembly method using water," ACS Appl. Mater. Interfaces 11, 33458–33464 (2019).
- ¹⁹P. B. Muller, R. Barnkob, M. J. H. Jensen, and H. Bruus, "A numerical study of microparticle acoustophoresis driven by acoustic radiation forces and streaming-induced drag forces," Lab Chip 12, 4617–4627 (2012).
- ²⁰D. G. Shchukin, E. Skorb, V. Belova, and H. Möhwald, "Ultrasonic cavitation at solid surfaces," Adv. Mater. 23, 1922–1934 (2011).
- ²¹N. Nama *et al.*, "Numerical study of acoustophoretic motion of particles in a PDMS microchannel driven by surface acoustic waves," Lab Chip **15**, 2700–2709 (2015)
- ²²L. Zhang and L. Liu, "Polymeric self-assembled monolayers anomalously improve thermal transport across graphene/polymer interfaces," ACS Appl. Mater. Interfaces 9, 28949–28958 (2017).
- ²³Z. Bai, L. Zhang, H. Li, and L. Liu, "Nanopore creation in graphene by ion beam irradiation: Geometry, quality, and efficiency," ACS Appl. Mater. Interfaces 8, 24803–24809 (2016).
- ²⁴A. S. Joshi and Y. Sun, "Wetting dynamics and particle deposition for an evaporating colloidal drop: A lattice Boltzmann study," Phys. Rev. 82, 041401 (2010).
- 25X. Kong et al., "Simulation of flow and soot particle distribution in wall-flow DPF based on lattice Boltzmann method," Chem. Eng. Sci. 202, 169–185 (2019).
 26S. T. W. Kuruneru, E. Sauret, S. C. Saha, and Y. T. Gu, "Coupled CFD-DEM simulation of oscillatory particle-laden fluid flow through a porous metal foam heat exchanger: Mitigation of particulate fouling," Chem. Eng. Sci. 179, 32–52 (2018)
- ²⁷H. Deponte *et al.*, "Experimental and numerical approach to resolve particle deposition on dimpled heat transfer surfaces locally and temporally," Chem. Eng. Sci. **227**, 115840, (2020).
- 286. C. Lee, W. G. Kim, and S. J. Yook, "Effect of plate thickness on particle deposition velocity onto a face-up flat plate situated parallel to an airflow," J. Appl. Phys. 110, 063518 (2011).
- ²⁹N. Nazemifard, J. H. Masliyah, and S. Bhattacharjee, "Particle deposition onto micropatterned charge heterogeneous substrates: Trajectory analysis," J. Colloid Interface Sci. 293, 1–15 (2006).
- ³⁰L. Liu and Y. Dzenis, "Simulation of electrospun nanofibre deposition on stationary and moving substrates," Micro Nano Lett. 6, 408–411 (2011).
- ³¹M. C. Chiou, C. H. Chiu, and H. S. Chen, "Modeling particle deposition from fully developed turbulent flow," Appl. Math. Model. **35**, 3238–3254 (2011).
- ³²M. Guingo and J. P. Minier, "A stochastic model of coherent structures for particle deposition in turbulent flows," Phys. Fluids **20**, 053303 (2008).
- ³³J. L. Galindo *et al.*, "Bulk characterization in a Monte Carlo particle-deposition model with a novel adherence-potential barrier," J. Appl. Phys. **120**, 034902 (2016).
- ³⁴H. Swenson and N. P. Stadie, "Langmuir's theory of adsorption: A centennial review," Langmuir 35, 5409 (2019).